

MESHLESS SOLUTION COMBINED WITH THE DRBEM FOR PLATE BUCKLING ANALYSIS

ALBERTO NUNES RANGEL¹, LEANDRO PALERMO JR¹ & LUIZ CARLOS WROBEL^{2,3}

¹School of Civil Engineering, Architecture and Urban Design, State University of Campinas, Brazil

²Department of Mechanical and Aerospace Engineering, Brunel University London, UK

³Department of Civil and Environmental Engineering, Pontifical Catholic University of Rio de Janeiro, Brazil

ABSTRACT

The application of the boundary element method to the buckling problem requires a domain integration and the use of the gradient boundary integral equation to perform the analysis. One of the most used techniques to convert the domain integral to equivalent boundary integrals is the dual reciprocity method (DRM). The present study employs the DRM in conjunction with a meshless solution using radial functions to obtain the gradient of the deflection instead of employing the gradient boundary integral equation. The plate bending model considered the effect of shear deformation and the results obtained are compared to those available in the literature.

Keywords: plates (engineering), boundary element method, buckling (mechanics).

1 INTRODUCTION

Plates have been incorporated to the principal structural elements in constructive and mechanical engineering systems, due to the improvement of the constructive processes. This feature has encouraged many researchers to develop theories to describe the bending behaviour of those elements, such as the Kirchhoff and the Reissner–Mindlin models [1], [2].

Although the plate bending behaviour can be appropriately defined with those models, only a few cases can be solved directly. The terms related to the geometrical non-linearity effect (GNL) in the buckling problem modifies the partial differential equations (PDE), and thus it becomes more difficult to obtain the exact solutions.

Some researchers on structural mechanics have developed many studies to analyse the plate buckling behaviour. To improve the accuracy on computation of the buckling parameters for the classical bending model, the minimum potential energy and the Rayleigh–Ritz method were employed by Bryan [3], for uniform compression cases, and by Way [4], for membrane shears combined to bending compression. Similar studies were done by Dawe and Roufaeil [5] and Xiang et al. [6], employing the Mindlin theory. Tham and Szeto [7] used the finite strip method (FSM) to obtain the first and the second buckling modes of square, triangular, parallelogrammatical and elliptical geometries. The finite element method (FEM) has been widely applied to plate buckling, like in Sakiyama and Matsuda [8] and Featherston and Ruiz [9]. The boundary element method (BEM) was used in the buckling analyses considering the classical bending model [10] or those with the effect of shear deformation in bending [11]. The boundary discretization is the main advantage of the BEM formulation, a small system of equations related to the boundary node values results in comparison to that in the domain discretization methods. The internal values required for the buckling analysis are subsequently computed after the solution of the system of equations. Nardini and Brebbia proposed the dual reciprocity method (DRM) [14] to keep the advantage of boundary only discretization in problems requiring the domain integral for the solution. The boundary integral equations of the problem are combined with the particular solutions used to convert the domain integrals in a sum of boundary integrals. The generalization of the DRM for several cases found in engineering problems as well as a complete explanation on the technique was done in Partridge et al. [15].



The dual reciprocity boundary element method (DRBEM) was used in problems containing the GNL effect, to compute the plate buckling parameters for rectangular and circular geometries [16], and to analyse large deflections of plates in Purbolaksono and Aliabadi [17], all of them based on the Reissner–Mindlin model. Considering the Kirchhoff's model, the DRBEM was combined with the analog equations method (AEM) in Chinnaboon et al. [18], to get the buckling factors of rectangular plates and in Katsikadelis and Babouskos [19] for post-buckling analysis. More complex applications using the multi-region method were done in Baiz and Aliabadi [20], on the local buckling of thin-walled structures using the classical model, on large deflections of assembled structures with shear deformable plates and in fracture mechanics including the GNL effect [22].

The present study is derived from Soares et al. [23] where the formulation for plate buckling considered the effect of shear deformation. No relation was required for in-plane stress derivatives and the GNL effect used the gradient of the deflection instead of the second derivatives of the deflection, requiring the null value for the divergence of the in-plane stress tensor, which is employed in most of the BEM formulations. The use of a meshless solution for the gradient of deflection instead of using the gradient boundary integral equation is the main difference in the present study with reference to Soares et al. [23]. The buckling parameter of unilaterally compressed square plates were obtained considering the simply supported and the clamped edge conditions for cases with thickness to plate side ratio between 0.001 to 0.2.

2 BOUNDARY INTEGRAL EQUATIONS

The linearization of the geometrical non-linearity (GNL) effect in the plate bending equilibrium under the in-plane forces on the domain results in the plate buckling equations [1]. The BEM formulation for the buckling analysis in isotropic plates [11] employed the displacement and the deflection gradient BIEs. The equations are next presented with the values $\{1, 2 \text{ and } 3\}$ for the Latin indices and $\{1, 2\}$ for the Greek indices. The differentiation in the kernels of the gradient BIE was written in terms of the field point coordinates:

$$C_{ij}(x')u_j(x') + \int_{\Gamma} [T_{ij}(x', x)u_j(x) - U_{ij}(x', x)t_j(x)]d\Gamma(x) = \dots$$

$$= \int_{\Gamma} n_{\alpha}(x)N_{\alpha\beta}(x)u_{3,\beta}(x)U_{i3}(x', x)d\Gamma(x) - \iint_{\Omega} N_{\alpha\beta}(X)u_{3,\beta}(X)U_{i3,\alpha}(x', X)d\Omega(X) \quad (1)$$

$$u_{3,\gamma}(X') = \int_{\Gamma} [T_{3j,\gamma}(X', x)u_j(x) - U_{3j,\gamma}(X', x)t_j(x)]d\Gamma(x) +$$

$$\dots - \int_{\Gamma} n_{\alpha}(x)N_{\alpha\beta}(x)u_{3,\beta}(x)U_{i3,\gamma}(X', x)d\Gamma(x) + \dots$$

$$\dots + \iint_{\Omega} N_{\alpha\beta}(X)u_{3,\beta}(X)U_{33,\alpha\gamma}(X', X)d\Omega(X) \quad (2)$$

where C_{ij} is an element of the matrix C related to the boundary geometry at the source point, being 0,5 for the external points and 1,0 for internal points, which becomes the identity matrix when a smooth boundary is considered, u_{α} is the plate rotation in direction α , and u_3 is the plate deflection. U_{ij} represents the rotation ($j = 1, 2$) or the deflection ($j = 3$) due to a unit couple ($i = 1, 2$) or a unit point force ($i = 3$). T_{ij} represents the moment ($j = 1, 2$) or the shear

($j = 3$) due to a unit couple ($i = 1, 2$) or a unit point force ($i = 3$). U_{ij} and T_{ij} are related to the fundamental solution. $N_{\alpha\beta}$ is the resultant on the thickness of the in-plane stresses.

The constitutive equations for the isotropic plates are given by:

$$M_{\alpha\beta} = D \frac{(1-\nu)}{2} \left(u_{\alpha,\beta} + u_{\beta,\alpha} + \frac{2\nu}{1-\nu} u_{\gamma,\gamma} \delta_{\alpha\beta} \right) \quad (3)$$

$$Q_\alpha = D \frac{(1-\nu)}{2} \lambda^2 (u_\alpha + u_{3,\alpha}) \quad (4)$$

with

$$\lambda^2 = 12 \frac{\kappa^2}{h^2}$$

D is the flexural rigidity, h is the plate thickness, ν is Poisson's ratio, and $\delta_{\alpha\beta}$ is the Kronecker delta. The shear parameter κ^2 is equal to $5/6$ or $\pi^2/12$ for the Reissner or the Mindlin model, respectively.

3 APPLICATION OF THE DUAL RECIPROCITY METHOD

The kernels in the domain integrals of eqns (1) and (2) contain the products between the GNL effect (plate deflection weighted by in-plane forces) and the first and the second derivatives of deflection due to the fundamental solution (U_{i3}), respectively. The introduction of the DRM in eqns (1) and (2) requires the use of the first derivative of the BIEs for the displacements (rotation and deflection) as well as the second derivatives of the BIE for the deflection [23].

$$u_{i,\gamma}(X') = \int_\Gamma [T_{ij,\gamma}(X', x) u_j(x) - U_{ij,\gamma}(X', x) t_j(x)] d\Gamma(x) - \iint_\Omega q(X) U_{i3,\gamma}(X', X) d\Omega(X) \quad (5)$$

$$u_{3,\alpha\gamma}(X') = \int_\Gamma [T_{ij,\alpha\gamma}(X', x) u_j(x) - U_{ij,\alpha\gamma}(X', x) t_j(x)] d\Gamma(x) - \iint_\Omega q(X) U_{i3,\alpha\gamma}(X', X) d\Omega(X) \quad (6)$$

The order of the singularities in eqns (1) and (2) are increased in the DRM with the introduction of eqns (5) and (6). The meshless formulation to obtain the gradient of the deflection carried to only use the eqn (3) in the DRM. In this way, the singularities remain in the same order of those in the formulation [11] with eqns (1) and (2). The gradient BIE (eqn 5) is introduced in eqn (3) to work with the DRM, which is combined with the meshless formulation.

The steps to introduce the DRM were the same in Soares et al. [23] but they were only applied to eqn (3). A vector function (b) related to the GNL effect and resulting from the product between the in-plane force tensor and the gradient of plate deflection is given by:

$$b_\theta(X) = N_{\theta\beta}(X) u_{3,\beta}(X) \quad (7)$$

The vector function (b) is approximated with the following relation [15]:

$$b_\theta(X) = \sum_{m=1}^{N+L} \alpha_\theta^m f^m \quad (8)$$

The summation in eqn (8) is extended to all points employed in the DRM, i.e., the total number of points placed on the boundary (N) and in the domain (L), f^m and α_θ^m are sets of the approximating functions and weighting coefficients, respectively [15]. The application of the DRM employs the particular solution \hat{u}_j^m , which is related to the approximating function f^m [23].

The radial basis function $(1 + r)$, which was used in Soares et al. [23], carried the following particular solutions:

$$\hat{u}_\alpha^m = \frac{1}{D} \left(\frac{r^3}{16} + \frac{r^4}{45} \right) r_{,\alpha} ; \quad \hat{u}_3^m = \frac{2}{D(1-\nu)\lambda^2} \left(\frac{r^2}{4} + \frac{r^3}{9} \right) - \frac{1}{D} \left(\frac{r^4}{64} + \frac{r^5}{225} \right) \quad (9)$$

The distributed shear and bending moments related to the particular solutions are obtained with the constitutive eqns (3) and (4), and reduced to the generalized tractions with the following relations:

$$\begin{aligned} \hat{t}_\alpha^m &= \hat{M}_{\alpha\beta}^m n_\beta \\ \hat{t}_3^m &= \hat{Q}_\beta^m n_\beta \end{aligned} \quad (10)$$

The displacement BIE for the buckling problem using the DRM is obtained after the introduction of the relation given in eqn (8) in the kernel of the domain integral in eqn (3) and using the gradient BIE, eqn (5). The final displacement BIE is given by Soares et al. [23]:

$$\begin{aligned} C_{ij}(x')u_j(x') + \int_{\Gamma} [T_{ij}(x',x)u_j(x) - U_{ij}(x',x)t_j(x)]d\Gamma(x) = \dots \\ = \int_{\Gamma} n_\alpha(x)N_{\alpha\beta}(x)u_{3,\beta}(x)U_{i3}(x',x)d\Gamma(x) + \sum_{m=1}^{N+L} \alpha_\theta^m \{c\hat{u}_{i,\theta}^m(x') + \dots \\ \dots \dots - \int_{\Gamma} [n_\alpha(x)M_{i\alpha\beta,\theta}(x',x)\hat{u}_\beta^m(x) + n_\beta(x)Q_{i\beta,\theta}(x',x)\hat{u}_3^m(x) + \dots \\ \dots - U_{i\beta,\theta}(x',x)\hat{t}_\beta^m(x) - U_{i3,\theta}(x',x)\hat{t}_3^m(x)]d\Gamma(x)\} \end{aligned} \quad (11)$$

The gradient of the deflection for the buckling analysis was obtained with the meshless formulation [15]. The meshless solution employed a different radial basis function to that in eqn (8) for the DRM. The relation between the deflection and the radial functions was established in the same way of eqn (8) and is given by:

$$u_3(X) = \sum_{m=1}^{N+L} \beta^m f_w^m \quad (12)$$

The gradient of the deflection considering eqn (12) is next written with the differentiation done on the radial basis function, i.e.:

$$u_{3,\theta}(X) = \sum_{m=1}^{N+L} \beta^m f_{w,\theta}^m \quad (13)$$

The gradient of the deflection is obtained when eqns (12) and (13) are combined, which can be written in the matrix form:

$$\begin{aligned} (u_3) &= [f_w](\beta) \Rightarrow (\beta) = [f_w]^{-1}(u_3) \\ (u_{3,\theta}) &= [f_{w,\theta}](\beta) \\ (u_{3,\theta}) &= [f_{w,\theta}][f_w]^{-1}(u_3) \end{aligned} \quad (14)$$

Two types of augmented thin plate spline RBF were employed in the numerical examples and are given by:

$$f_w^m = \left(\frac{r}{c}\right)^4 \ln \left[1 + \frac{r}{c} + \left(\frac{r}{c}\right)^2 + \left(\frac{r}{c}\right)^3 \right] \quad (15)$$

$$f_w^m = \left(\frac{r}{c}\right)^3 \ln \left[1 + \frac{r}{c} + \left(\frac{r}{c}\right)^3 + \left(\frac{r}{c}\right)^5 \right] \quad (16)$$

4 NUMERICAL IMPLEMENTATION

The discretization of the BIEs employed quadratic isoparametric boundary elements with the collocation points always placed on the boundary. The same mapping function was used for conformal and non-conformal interpolations. The collocation points were placed at positions $(-0.67$ and $0.0)$, in the range $(-1, +1)$, in the case of continuous elements and at positions $(-0.67, 0.0, +0.67)$ in the case of discontinuous elements, i.e., the collocation points were always shifted inside the boundary elements. The singularity subtraction [13] and the transformation of variable techniques [13] were employed for the Cauchy and weak-type singularities, respectively, when integrations were performed on elements containing the collocation points. The standard Gauss–Legendre scheme was employed for integrations on elements not containing the collocation points.

The DRM considered points distributed in the domain and on the boundary. The points on the boundary were placed at the positions of the collocation points. The first boundary integral on the right-hand side (RHS) of eqn (11) is not related with the DRM but the result of the algebraic manipulation on the integral containing the GNL effect in Soares and Palermo [11]. The discretization of the DBIE in eqns (1) or (11) assumed a constant value along each boundary element for the sum of products between the gradient of the deflection and the in-plane forces, which values were obtained at the central node of the boundary elements. It is necessary to note the value the deflection gradient was computed with eqn (14) in this study.

The eigenvalue analysis used the basic inverse iteration with the Rayleigh quotient [23] according to the following equations:

$$Ax^{(k+1)} = Bx^{(k)} \quad (17)$$

$$\lambda_k = \frac{(x^{(k+1)}, x^{(k)})}{(x^{(k+1)}, x^{(k+1)})} \quad (18)$$

The vector $x^{(k)}$ in eqns (17) and (18) is related to values of the gradient of the deflection at the DRM points. Starting with an eigenvector $x^{(0)}$ with elements equal to 1.0, the values of the displacements and tractions at the boundary nodes are found with eqn (11), and the deflection values are introduced in eqn (14) to get the gradients, which were used to obtain the eigenvector $x^{(1)}$. The vectors $x^{(0)}$ and $x^{(1)}$ are introduced in eqn (18) to obtain the eigenvalues.

5 NUMERICAL EXAMPLES

A square plate under uniform load on the domain was solved and the results obtained with the meshless solution (eqn 14) were compared with the BEM solution (eqn 5) [12]. The Young's modulus (E) and Poisson's ratio (ν) were 2 MPa and 0.3, respectively. The shear parameter κ^2 was $\pi^2/12$ (Mindlin), the plate side (L) and thickness (h) were 4 m and 0.8 m, respectively, and the uniform load q was 0.64 kN.m^{-2} . The boundary conditions were the clamped edge (C), the free edge (F) and the simply supported edge (S) with the hard condition (the twist rotation restrained). The meshes used 128 quadratic boundary elements (BE) combined with 49 internal points (P) uniformly distributed in the domain, 121 (P) and 225 (P). The results obtained with 49 internal points are presented because better values were obtained when the number of internal points was increased. The radial function for the meshless solution was presented in eqn (15). The relative differences between the obtained results are presented in Tables 1 and 2. The relative differences were increased in cases with free edges.



Table 1: Relative differences between results obtained for deflection gradient with the BEM solution (eqn 5) and the meshless solution (eqn 14) for plates with same boundary conditions on opposite sides.

Position		Relative differences (%)									
x_1/L	x_2/L	$u_{3,1}$	$u_{3,2}$	$u_{3,1}$	$u_{3,2}$	$u_{3,1}$	$u_{3,2}$	$u_{3,1}$	$u_{3,2}$	$u_{3,1}$	$u_{3,2}$
0.125	0.125	0.8	0.8	1.1	1.1	2.3	1.6	9.3	0.3	14.7	1.6
0.250	0.125	0.4	0.2	0.6	2.0	1.4	2.7	6.7	0.3	1.5	0.6
0.375	0.125	0.3	0.0	0.4	2.3	1.1	3.1	5.7	0.2	1.3	0.3
0.500	0.125	—	0.0	—	2.4	—	3.1	—	0.2	—	0.2
0.125	0.250	0.2	0.4	2.0	0.6	1.1	0.8	6.7	0.1	30.6	0.6
0.250	0.250	0.1	0.1	0.9	0.9	0.8	1.2	5.1	0.1	19.5	0.3
0.375	0.250	0.1	0.0	0.7	1.1	0.6	1.4	4.5	0.1	16.5	0.1
0.500	0.250	—	0.0	—	1.1	—	1.4	—	0.1	—	0.1
0.125	0.375	0.0	0.3	2.3	0.4	0.8	0.6	5.5	0.1	25.4	0.3
0.250	0.375	0.0	0.1	1.1	0.7	0.5	0.9	4.1	0.1	21.2	0.2
0.375	0.375	0.0	0.0	0.7	0.7	0.4	0.9	3.6	0.1	19.6	0.1
0.500	0.375	—	0.0	—	0.8	—	1.0	—	0.1	—	0.1
0.125	0.500	0.0	—	2.4	—	0.7	—	5.2	—	23.1	—
0.250	0.500	0.0	—	1.1	—	0.4	—	3.9	—	20.0	—
0.375	0.500	0.0	—	0.8	—	0.3	—	3.4	—	19.1	—
0.500	0.500	—	—	—	—	—	—	—	—	—	—
Boundary conditions		SSSS		CCCC		CSCS		SFSS		CFCF	

Table 2: Relative differences between results obtained for deflection gradient with the BEM solution (eqn 5) and the meshless solution (eqn 14) for plates with same boundary conditions on opposite sides in one direction only.

Position		Relative differences (%)			
x_1/L	x_2/L	$u_{3,1}$	$u_{3,2}$	$u_{3,1}$	$u_{3,2}$
0.125	0.125	15.1	1.9	0.7	2.4
0.375	0.125	24.8	0.1	0.3	2.8
0.625	0.125	25.2	0.1	0.3	2.8
0.875	0.125	15.3	1.9	0.7	2.4
0.125	0.375	2.3	0.1	0.2	0.3
0.375	0.375	1.9	0.0	0.1	0.4
0.625	0.375	1.5	0.0	0.1	0.4
0.875	0.375	1.9	0.1	0.2	0.3
0.125	0.625	4.7	0.0	0.0	0.7
0.375	0.625	2.4	0.0	0.0	0.4
0.625	0.625	2.3	0.0	0.0	0.4
0.875	0.625	4.5	0.0	0.0	0.6
0.125	0.875	4.4	0.2	0.2	4.3
0.375	0.875	1.6	0.1	0.0	2.9
0.625	0.875	1.6	0.1	0.0	2.9
0.875	0.875	4.4	0.2	0.2	4.2
Boundary conditions		CFFF		CSFS	

The buckling parameters were obtained for a square plate under uniaxial compression condition shown in Fig. 1, considering the simply supported and clamped edge conditions, and using 128 quadratic boundary elements and 676 internal points. The results obtained for those cases are presented in Table 3, and were very close to the literature. They are shown to evaluate the application of the meshless solution combined with the DRM for a non-linear problem. The buckling parameter k is a non-dimensional value related to the critical load of the plate (N_{cr}), the length of the plate side (a) and the flexural rigidity (D) according to following expression:

$$k = \frac{a^2 N_{cr}}{\pi^2 D} \quad (19)$$



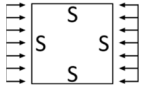
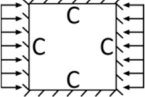
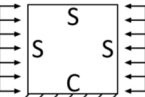
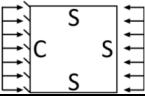
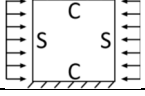
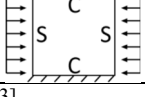
Figure 1: Square plate under uniaxial compression.

The plates had a thickness to length ratio between 1/1000 and 1/5. The Young's modulus (E) and Poisson's ratio (ν) were 206.9 GPa and 0.3, respectively. The value of the shear parameter κ^2 was 5/6. The comparison between values for the buckling parameter obtained with the results available literature are presented in Table 1.

6 CONCLUSIONS

The present technique combining the DRM to convert the domain integral to equivalent boundary integrals and the meshless solution to compute the deflection derivatives instead of using the BIE for the gradient of the deflection was efficient to compute the buckling parameters. The displacement BIE containing terms resulting from the DRM was the only equation in the numerical formulation. The equation was used to obtain the boundary element matrices as in all boundary element formulations and to compute the required deflection at the points needed to obtain the gradient of the deflection, which is used to introduce the GNL effect. The main feature with reference to the formulation presented in Soares et al. [23] was the use of one equation type (displacement BIE) in the solution instead of working with the gradient BIE containing integrals with the singularities increased. The computer and/or numerical effort in this technique was low whereas the choice of the better radial function to perform an efficient analysis was the main difficulty. The authors intend to apply the present technique to all cases studied in Soares and Palermo [11] and Soares et al. [23] and relevant cases in the literature.

Table 3: Buckling parameters for the square plate obtained with the DRM combined with the meshless solution for the deflection derivatives.

Type	h/a	[21]	Obtained	Difference (%)
1. SSSS 	0.001	4.0000*	4.0931	2.328
	0.01	3.9977	3.9972	0.013
	0.05	3.9444*	3.9448	0.010
	0.100	3.7865*	3.7868	0.008
	0.200	3.2637*	3.2639	0.006
2. CCCC 	0.01	10.1382*	10.0464	0.905
	0.05	9.5588*	9.5666	0.082
	0.1	8.2917*	8.2993	0.092
	0.2	5.3156*	5.3448	0.549
3. CSSS 	0.001	5.7401	5.7516	0.200
	0.05	5.5977	5.6003	0.046
	0.100	5.2171	5.2238	0.128
	0.200	4.1364	4.1514	0.363
4. SSSC 	0.001	4.8471	4.9969	2.013
	0.05	4.7454	4.7495	0.086
	0.1	4.4656	4.4724	0.152
	0.2	3.6115	3.6254	0.385
5. CSCS 	0.001	7.6911	7.6880	0.040
	0.05	7.2989	7.3109	0.164
	0.1	6.3698	6.3896	0.311
	0.2	4.3204	4.3480	0.639
6. CSCS 	0.001	6.7431	6.5317	3.135
	0.05	6.5238	6.5316	0.120
	0.1	5.9487	5.9626	0.234
	0.2	4.4004	4.4243	0.543

*[23]

REFERENCES

- [1] Timoshenko, S. & Woinowsky-Krieger, S., *Theory of Plates and Shells*, McGraw-Hill: New York, 1959.
- [2] Timoshenko, S. & Gere. J., *Theory of Elastic Stability*, New York: McGraw-Hill, vol. 294, 1961.
- [3] Bryan, G.H.. On the Stability of a plane plate under thrusts in its own plane, with applications to the “buckling” of the sides of ship. *Proceedings of the London Mathematical Society*, **1**(1), pp. 54–67, 1890.
- [4] Way, S., Stability of rectangular plates under shear and bending forces. *Journal of Applied Mechanics*, **16**, 1936.
- [5] Dawe, D.J. & Roufaeil, O.L., Buckling of rectangular Mindlin plates. *Computers and Structures*, **15**(4), pp. 461–471, 1982.
- [6] Xiang, Y. et al., Mindlin plate buckling with prebuckling in-plane deformation. *Journal of Engineering Mechanics*, vol. 119, n. 1. pp. 1–18, 1993.
- [7] Tham, L. & Szeto, H., Buckling analysis of arbitrarily shaped plates by spline finite strip method. *Computers and Structures*, **36**(4), pp. 729–735, 1990.



- [8] Sakiyama, T. & Matsuda, H., Elastic buckling of rectangular Mindlin plate with mixed boundary conditions. *Computers and Structures*, **25**(5), pp. 801–808, 1987.
- [9] Featherson, C.A. & Ruiz, C., Buckling of flat plates under bending and shear. Department of Engineering Science, University of Oxford, 1998.
- [10] Bezine, G., Cimetiere, A. & Gelbert, J.P., Unilateral buckling of thin elastic plates by the boundary integral equation method. *International Journal for Numerical Methods in Engineering*, **21**(12), pp. 2189–2199, 1985.
- [11] Soares Jr., R.A. & Palermo Jr., L., Effect of shear deformation on the buckling parameter of perforated and non-perforated plates studied using the boundary element method. *Engineering Analysis with Boundary Elements*, **85**, pp. 57–69, 2017.
- [12] Weeën, F.V., Application of the boundary integral equation method to Reissner's plate model. *International Journal for Numerical Methods in Engineering*, **18**(1), pp. 1–10, 1982.
- [13] Wrobel, L.C., *The Boundary Element Method: Applications in Thermo-Fluids and Acoustics*. John Wiley: Chichester, UK, 2002.
- [14] Nardini, D. & Brebbia, C.A., A new approach to free vibration analysis using boundary elements. *Applied Mathematical Modelling*, **7**(3), pp. 157–162, 1983.
- [15] Partridge, P.W., Brebbia, C.A. & Wrobel, L.C., *The Dual Reciprocity Boundary Element Method*, Computational Mechanics Publication and Elsevier Applied Science: London and New York, 1992.
- [16] Purbolaksono, J. & Aliabadi, M.H., Buckling analysis of shear deformable plates by boundary element method. *International Journal for Numerical Methods in Engineering*, **62**, pp. 537–563, 2004.
- [17] Purbolaksono, J. & Aliabadi, M.H., Large deformation of shear deformable plate by boundary element method. *Journal of Engineering Mathematics*, **51**, pp. 211–230, 2005.
- [18] Chinnaboon, B., Chucheepsakul, S. & Katsikadelis, J.T., A BEM-based meshless method for elastic buckling analysis of plates. *International Journal of Structural Stability and Dynamics*, **7**(1), pp. 81–99, 2007.
- [19] Katsikadelis, J.T. & Babouskos, N., The post-buckling analysis of plates: A BEM based meshless variational solution. *Automatic Control and Robotics*, **6**, pp. 113–118, 2007.
- [20] Baiz, P.M. & Aliabadi, M.H., Local buckling of thin-walled structures by the boundary element method. *Engineering Analysis with Boundary Elements*, **33**(3), pp. 302–313, 2009.
- [21] Hosseini-Hashemi, S., Khorshidi, K. & Amabili, M., Exact solution for linear buckling of rectangular Mindlin plates. *Journal of Sound and Vibration*, **315**(1), pp. 318–342, 2008.
- [22] Purbolaksono, J., Dirgantara, T. & Aliabadi, M.H., Fracture mechanics analysis of geometrically nonlinear shear deformable plates. *Engineering Analysis with Boundary Elements*, **36**, pp. 87–92, 2012.
- [23] Soares Jr., R.A., Palermo Jr., L. & Wrobel, L.C., Application of the dual reciprocity method for the buckling analysis of plates with shear deformation. *Engineering Analysis with Boundary Elements*, **106**, pp. 427–439, 2019.

